Pont de Pierre of Bordeaux Data Monitoring Analysis: Applications of HST and BDLM Models and Benefits for Reinforcement Works

Valdeyron Gilles, *Geotechnical Engineer, Cerema, Bordeaux (France); email: gilles.valdeyron@cerema.fr*

ABSTRACT: *The Pont de Pierre of Bordeaux, France, built between 1810 and 1821, was the first bridge erected across the Garonne in Bordeaux. Since the beginning of the construction, each pier of the bridge is affected by excessive settlements. Six of them (Piers 1 to 6) have even been reinforced by micropiles in 1993-1994 (Piers 1 to 4) and 2002 (Piers 5 and 6). The settlement and overtopping measurements available before and after reinforcement are analyzed using two complementary models (Hydrostatic Season Time and Bayesian Dynamic Linear Model) to highlight the benefits of the work and analyze the effect of external stresses on the structure. Moreover, data analysis provides a convincing tool for detecting anomalies during reinforcement and maintenance works.*

KEYWORDS: Bayesian Dynamic Linear Model, Hydraulic Season Time, Monitoring, Bridge, Masonry, Underpinning

SITE LOCATION: Geographic Database

INTRODUCTION

Historical, Structural and Geotechnical Context

The Stone Bridge, illustrated in Figure 1, is 486 m long and composed of two abutments (CRG and CRD) on each side and 17 low masonry arches with an average span of 23 m. All piers (P01 to P16) are founded on the Garonne River. The ascending order for the piers' numbering is from left (CRG) to right (CRD) on the river border side. From top to bottom, the ground foundation is composed by recent alluvial deposits (silty clays or silty sands); below, a layer of coarse sand and gravel is encountered, which is underlain by marls and limestone substratum. The upper layer is getting less and less clayey and thinner from the left to the right border of the Garonne (see Figure 2). Due to poor mechanical properties of the upper layer of the ground foundation, each pier and its abutments are founded on approximatively 250 wooden piles anchored in the sand and gravel layer. On the left border of the Garonne (that concerns the left abutment and Piers 1 to 4), driven wooden piles were installed with lower energy than the others, indicating a weaker anchorage of piles. Aware of the difficulties to ensure a perennial foundation for the bridge, designers have constructed a system of inside arches in each pier to reduce their weight. Theoretically, this results in a complex behaviour between an arch bridge and a box girder bridge. Moreover, a tramway platform, made of a concrete slab, has been added on the extrados bridge; this tramway warrants further consideration.

Due to its vicinity to the Atlantic Ocean, the bridge is submitted to the tide cycles; the average variation of the Garonne's water level is about 5 m. Each cycle takes about 12:25 hours and consists of two high and two low tides per day. This implies a cyclic action on the wooden piles foundations, due to flotation, of about 5 m, which is equivalent to a 10% variation of the load on each pier and abutments foundation. Indeed, at high tide, due to buoyancy, permanent loads on foundations are reduced and the loading of the foundations is maximum at low tide. Additionally, the bridge is affected by scours on the piers' sides but also in front of and beside the bridge, where sub-river slopes draw up to the foundations.

Submitted: 01 July 2024; Published: 30 October 2025
Reference: Valdeyron G. (2025). *Pont de Pierre of Bordeaux Data Monitoring Analysis: Applications of HST and BDLM Models and Benefits for Reinforcement Works.* International Journal of Geoengineering Case Histories, Volume 8, Issue 3, p. 29-53, doi: 10.4417/IJGCH-08-03-03

Since the beginning of construction, the bridge has been affected by excessive settlements, notably explained by a weaker anchorage of piles, and the left border was the first to be affected (Piers 1 to 4). Before reinforcement by micropiles, the settlement rate of Piers 1 to 4 was about 4 to 20 mm per year, and 1.5 to 3 mm/year for Piers 5 and 6 (see Figure 3).
Differential settlements led to structural damages as fractures on internal arches and piers. P02 and P03 were the first piers to be affected as far back as 1860, by a through fracture on the shaft of about 15 mm for P02, as can be seen in Figure 4. Since then, the other piers were also affected.

Figure 1. The Pont de Pierre of Bordeaux.

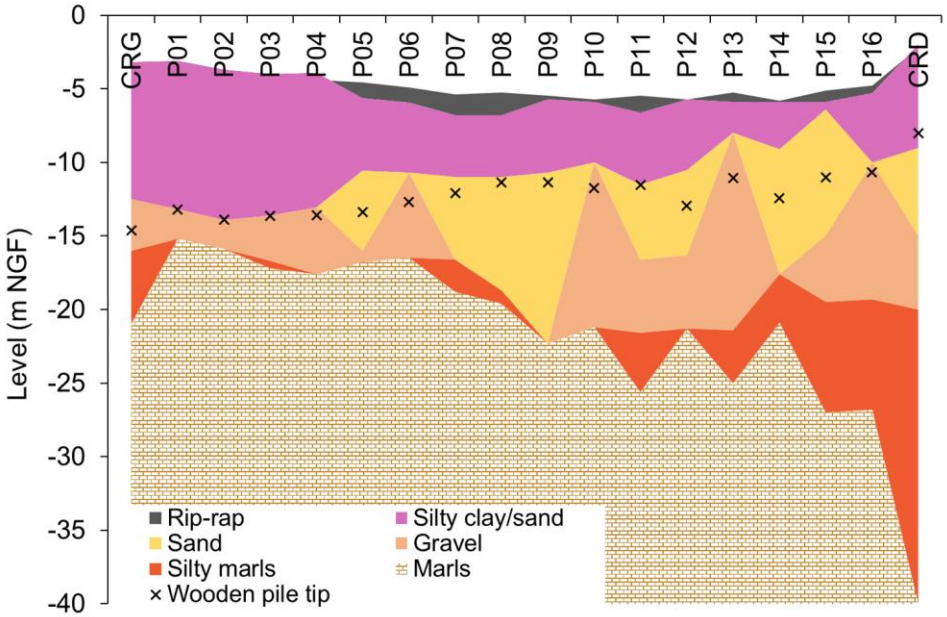

Figure 2. Geotechnical longitudinal profile.

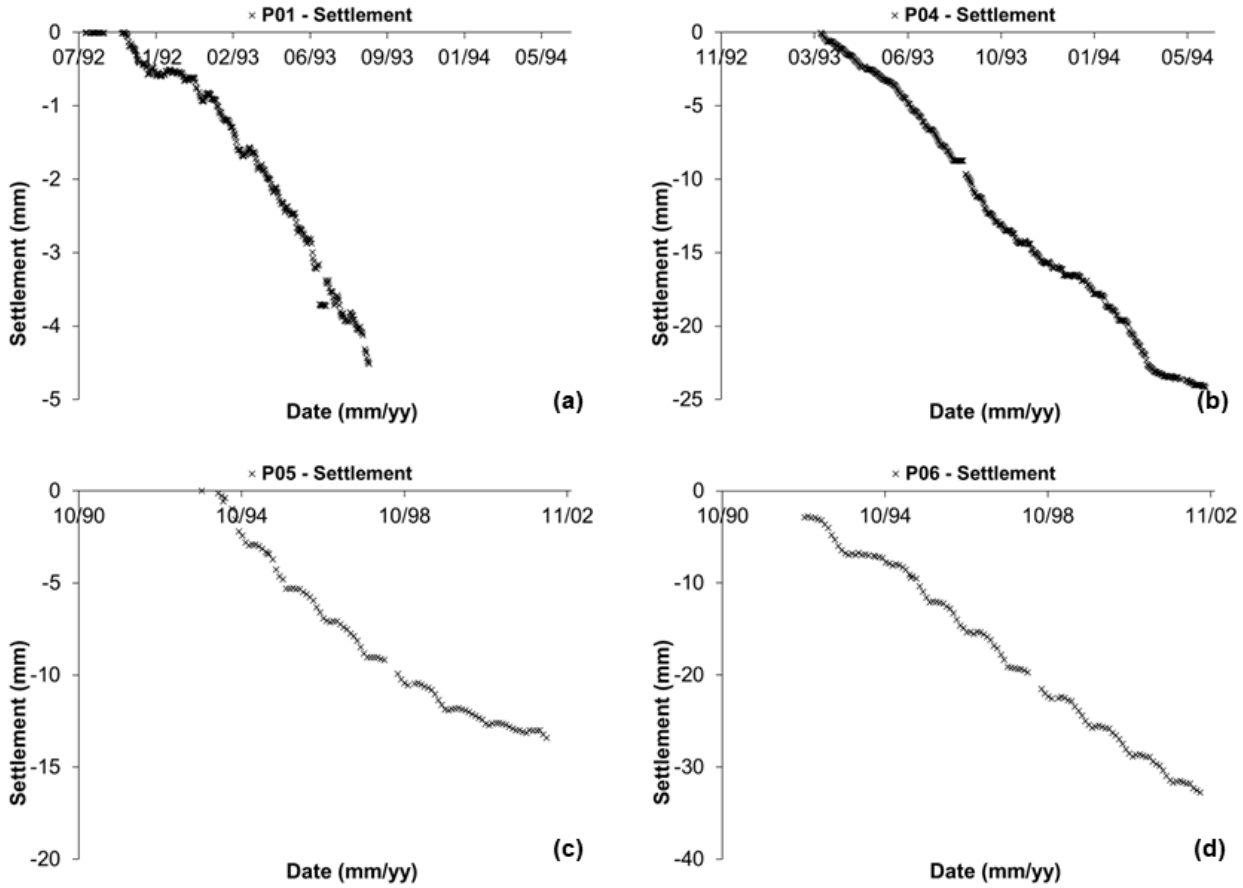

Figure 3. Settlement curves before reinforcement: (a) P01, (b) P04, (c) P05, and (d) P06.

Figure 4. Fracture on P02, illustrated on the left (1860, departmental archives) and pictured on the right (2014).

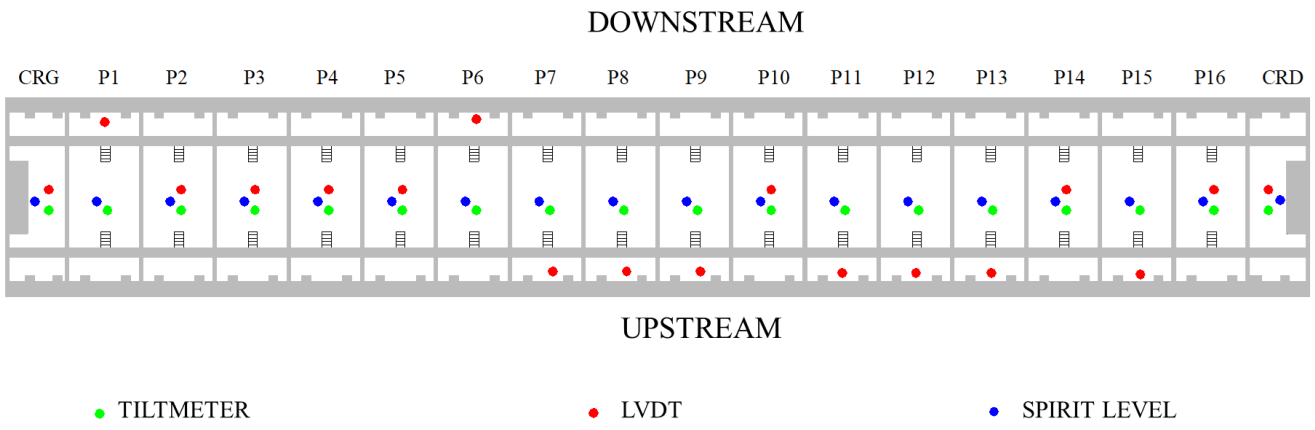

Figure 5. Schematic of sensor layout on the bridge.

Description of Available Data Monitoring

A first monitoring system constituted of a fixed-point system (Valdeyron et al., 2023), acting like an inverse pendulum that was set up to measure the piers' settlements of P10 and P14 in 1982, then of P16 in 1983, and of P02 and P03 in 1985. Finally, in 1991-92, this system was extended to all 16 piers and two abutments and completed by 18 tiltmeters. In 2003, a complete restoration of the monitoring system was realized and is still used nowadays.

Between 1982 and 2002, the settlements of each pier and abutment were measured with a variable measurement time step (1 measurement per half hour to 1 measurement/month). A new monitoring system was implemented in 2003 in order to measure settlements and tilting. This new monitoring system is composed by 18 (one on each pier and abutment) highly precise inductive displacement transducers (LVDT). In addition, 18 tiltmeters have been installed to measure the upstream/downstream inclination (see Figure 5). By default, the time step is 1 measurement per hour; during works on the bridge, however, this time step was increased to 4 measurements per hour in order to enhance the analyses of data monitoring and relationships with works. The accuracy of the settlement gauges is 1 µm and 10^{-5} rad for the tiltmeters.

There is no direct level measurement of tide level on the bridge; tide levels are measured by tide gauges, located 4 km downstream from the bridge in the Bordeaux harbor.

Some underpinned micropiles (4 of 16) of Piles 1 to 6 were monitored by stress gauges in order to measure the load transfer process from the wooden pile foundation to the micropiles.

In 1992 and 1993, thermal captors were set up on P01 and Arch 2 (between P01 and P02) in order to understand the thermal behavior of the bridge (see Figure 14).

Description of Works

The edge of each pillar is covered with rockfill to provide protection against scour. The protection of the bridge against scour was one of the main concerns of the designers. Claude Deschamps, designer of the bridge and Engineer, explains: "This monument will remain standing as long as the engineers take care of the rockfill protection." Indeed, the rockfill was backfilled in 1901, 1928, 1939, 1967, 1987, 1993, 1995-97, and 2018 (illustrated in Figure 6d).

As explained, fractures on the piers had to be treated by a post-tensioning system around the mansonry. P02 and P03 were the first reinforced piers in 1910 (the second intervention was made in 1993), then P04 was reinforced in 1988, P01 in 1993, and finally P05 and P06 in 2002 (see Figure 6a). The required tension was 600 kN for P03 and 400 kN for the other piers.

In 1954, the bridge was widened using reinforced concrete caissons in order to ensure the smooth passage of traffic (cars and pedestrians).

Figure 6. Illustration of works: (a) Post-tensioning on P05 and P06, (b) Micropiles on P05 and P06, (c) driven dolphins works on P08 and P09 (source: Bernard Tocheport), (d) rip-rap works on whole bridge (source: Sud-Ouest).

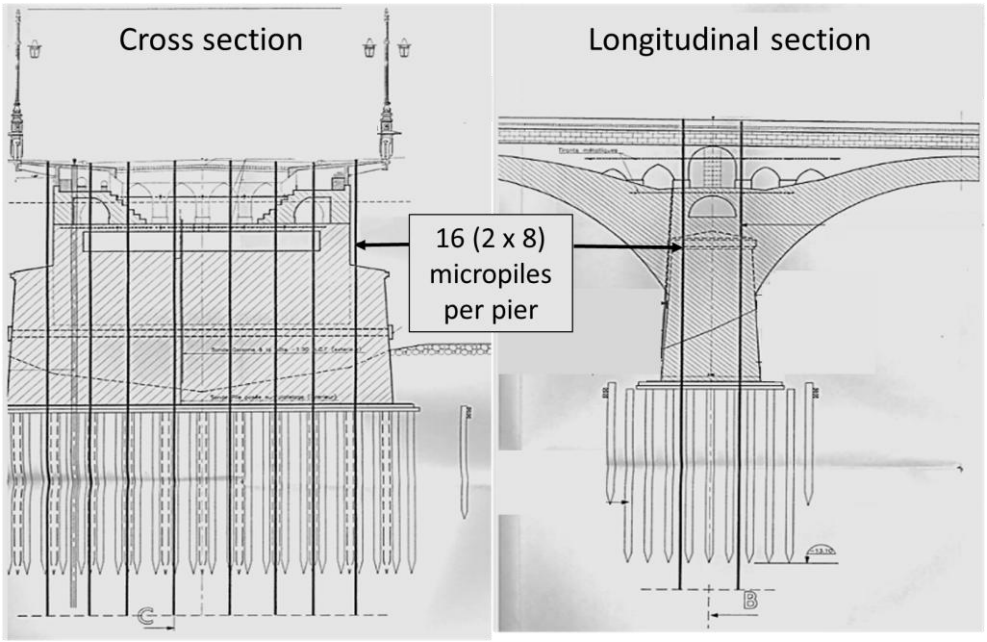

Figure 7. Principle of micropiles reinforcement in transversal (left) and longitudinal section (center).

The first foundations' reinforcements were realized in 1992-94 on piers P01 to P04 by sealing the masonry and anchoring in the marls with a set of 16 micropiles per pier (two lines of eight micropiles). The aim was to provide additional resistance to the wooden piles' foundations in order to limit settlements. Then in 2002-03, P05 and P06 were treated with the same process (Figure 6b). The design of these reinforcement is illustrated in Figure 7.

In 2003, a tramway infrastructure, consisting of railways laid on a renforced concrete slab and electric floor alimentation, was installed on the bridge in order to connect both sides of the Garonne. In order to protect the bridge against Airbus barge impact, mooring dolphins were driven in the vicinity of P08 and P09 in 2004 (see Figure 6c).

Geotechnical investigations were carried out from April to July 2021 throughout the piers and the foundations of Piers 7 to 16, and the abutments and two micropile tests were bored and sealed on Pier 8 in October 2022.

HYDROSTATIC SEASON TIME (HST) AND BAYESIAN DYNAMIC LINEAR MODELS: A SHORT REVIEW OF THEORETICAL ASPECTS

The Hydrostatic-Season-Time (HST) model

The tools most commonly used for dam monitoring data analysis purposes are the statistical methods of the Hydrostatic-Season-Time (HST) type. These methods were first developed in the 1960s to analyze the displacements resulting from the pendulum effects occurring at arch dams (Ferry and Willm, 1958). They are still being used in several countries to analyze measurements of other kinds (Guedes and Coehlo, 1985; Carrère et al., 2000; Bonelli, 2008 and 2009). The HST model is based on effects of three kinds. First, there are the hydrostatic effects, which correspond to the variations H resulting from changes in the water level. This variable is given by a polynomial of order 4 (parameters a_1, a_2, a_3, a_4):

$$H(t) = a_1 z(t) + a_2 z^2(t)) + a_3 z^3(t) + a_4 z^4(t) \quad (1)$$

With $z(t) = (Z(t) - Z_{min})/(Z_{max} - Z_{min})$, where $Z(t)$ is the reservoir level (minimum value Z_{min}, maximum value Z_{max}).

$z(t)$ is variyng between 0 to 1.

The second term is the time of year, which accounts for seasonal variations S in the measurements during twelve-month and six-month periods, and is described by the following expression (parameters A_1, d_1, A_2, d_2):

$$S(t) = A_1 sin(\omega_a(t - d_1)) + A_2 sin(2\omega_a(t - d_2)) \quad (2)$$

where $\omega_a = 2\pi/T_a$ is the annual angular frequency (T_a corresponds to a one-year period), and d_1 and d_2 represent the lag times (phase shifts).

The seasonal variations effect, assumed to be reversible, is quantified by maximum amplitudes A_i and lag time d_i. One of the oldest known applications of this model was developed by Forbes (1846), who used the so-called "sinusoidal adjustment method" to account for cyclic variations in soil temperature.

The third term accounts for the time-dependent trends in the ageing processes. This variable is often called the "irreversible effect". It is expressed as follows (parameters c_1, c_2, c_3):

$$T(t) = c_1\tau + c_2 exp(\tau) + c_3 exp(-\tau) \quad (3)$$

with $\tau = (t - t_0)/\Delta T$, where t is time, and $[t_0, t_0 + \Delta T]$ is the analysis interval. The settlement rate is given by the time derivative, estimated in the middle of the analysis interval:

$$v_1 = [c_1 + c_2 exp(1/2) - c_3 exp(-1/2)]/\Delta T \quad (4)$$

The HST model $Y(t) = Y_0 + H(t) + S(t) + T(t)$ has 11 parameters estimated by a multiple linear regression with MSE $||y - Y||^2$ where y is the measurement. This approach has been classically used to analyze dam monitoring data. The experience acquired at several hundreds of dams has confirmed what an excellent tool this approach can be for interpreting

monitoring data. It has also been used in many other fields (Young, 1998). In the present work, the HST model is applied to vertical displacement analysis measured on the Pont de Pierre.

Initial application of the HST Model was for dam engineering where the variable H results from the water level variation of the reservoir. In our case, to take into account that high water level has a positive effect on settlements (due to buoyancy, as previously explained), the H variable is modified by the way of $z(t)$ to:

$$z(t) = \left[\left(G(t) - W(t)\right)_{max} - \left(G(t) - W(t)\right)\right] / \left[\left(G(t) - W(t)\right)_{max} - \left(G(t) - W(t)\right)_{min}\right] \quad (5)$$

Where $G(t)$ is the permanent load of the pier and $W(t)$ is the buoyancy force due to tide water level variations. Thus, $z(t)$ is the loading ratio of the foundation; it equals 1 at minimum measured low tide level and 0 at maximum measured high tide.

The Bayesian Dynamic Linear Model (BDLM)

Initially and mainly used in econometrics, BDLM has been recently developed for Structural Health Monitoring issues. In this paper, all analyses have been carried out with the practical open-source software for a time series analysis called OpenBDLM (Gaudot, 2019). Theoretical aspects are extensively exposed in the bibliography (Goulet, 2017 and 2018) and can be briefly summarized as follows:

Observations $\boldsymbol{y}_t$ (for example, settlement measurements) are described, for each time t between 1 and T, by a superposition of hidden states $\boldsymbol{x}_t$:

$$\boldsymbol{y}_t = \boldsymbol{C}_t \boldsymbol{x}_t + \boldsymbol{v}_t, \begin{cases} \boldsymbol{y}_t \sim \mathcal{N}(\mathbb{E}[\boldsymbol{y}_t], cov[\boldsymbol{y}_t]) \\ \boldsymbol{x}_t \sim \mathcal{N}(\boldsymbol{\mu}_t, \boldsymbol{\Sigma}_t) \\ \boldsymbol{v}_t \sim \mathcal{N}(0, \boldsymbol{R}_t) \end{cases} \quad (6)$$

Where $\boldsymbol{C}_t$ is an observation matrix which indicates which hidden state contributes to the observations, and $\boldsymbol{v}_t$ is the observations error. Each quantity is supposed to be a Gaussian random variable. A transition model permits us to associate the variation of the hidden states at time t knowing the value between 1 and t-1, and this transition model is described by a matrix $\boldsymbol{A}_t$. A transition model error $\boldsymbol{Q}_t$ is also associated to $\boldsymbol{A}_t$:

$$\boldsymbol{x}_t = \boldsymbol{A}_t \boldsymbol{x}_{t-1} + \boldsymbol{w}_t, \ \boldsymbol{w}_t \sim \mathcal{N}(0, \boldsymbol{Q}_t) \quad (7)$$

A BDLM is built by representative blocks of different possible behaviors, generally $\boldsymbol{x}_t$, that can be handled with a combination of:

- Local Level (LL): baseline response of the structure;
- Local Trend or Local Acceleration (LT or LA): linear or accelerated response of the structure (for example, the ageing component of the structure);
- Periodic: harmonic component, such as seasonal effects;
- Auto-Regressive component: time-dependent model prediction errors (what is not caught by previous components).

For example, considering the Local Level block:

$$\boldsymbol{x}^{LL} = x^{LL}, \boldsymbol{A}^{LL} = 1, \boldsymbol{C}^{LL} = 1, \boldsymbol{Q}^{LL} = (\sigma^{LL})^2 \quad (8)$$

Where σ^{LL} is the model error term.

The aim of BDLM is to forecast the structure response at time $t+n$ ($\boldsymbol{y}_{t+n}$) beyond the current time t. To do that, a Kalman filter algorithm, divided in two parts (the prediction step and the measurement step) is used. In the prediction step, the probability hidden state values $\boldsymbol{x}_t$ at time t, is calculated on the basis of a set of known observations $\boldsymbol{y}_{t-1}$ between 1 and t-1. In the measurement step, $\boldsymbol{y}_t$ is used in order to correct the estimation previously given. Then, optimization of the model parameters is given by the technique of Maximum Likelihood Estimation, which seeks the maximization of the logarithm of the prior probability of the observation $\boldsymbol{y}_t$ at time t knowing the state estimated at time t-1 (prediction step).

RESULTS OF THE COMPARATIVE ANALYSIS OF BRIDGE BEHAVIOUR BEFORE AND AFTER REINFORCEMENT

Effects of Micropile Reinforcement on Settlements

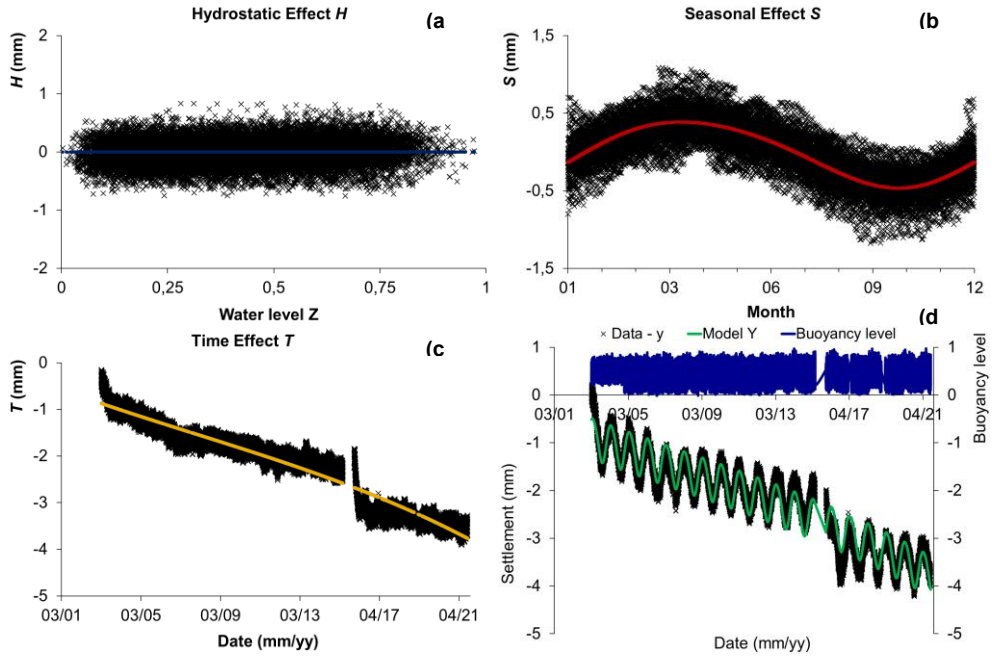

Figure 8. Results of the HST analysis of P02 measurements in 2003-21 (after reinforcement): (a) Hydrostatic effect H, (b) Seasonal effect S, (c) Time effect T, and (d) Data, model and buoyancy level.

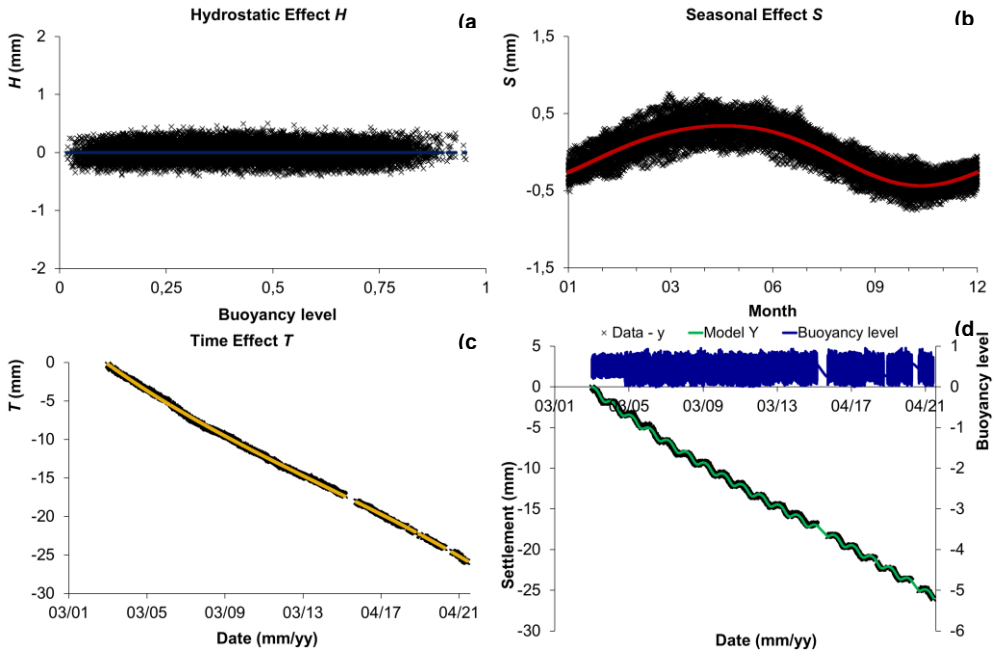

Figure 9. Results of the HST analysis of P14 measurements in 2003-21 (before reinforcement): (a) Hydrostatic effect H, (b) Seasonal effect S, (c) Time effect T, (d) Data, model and buoyancy level.

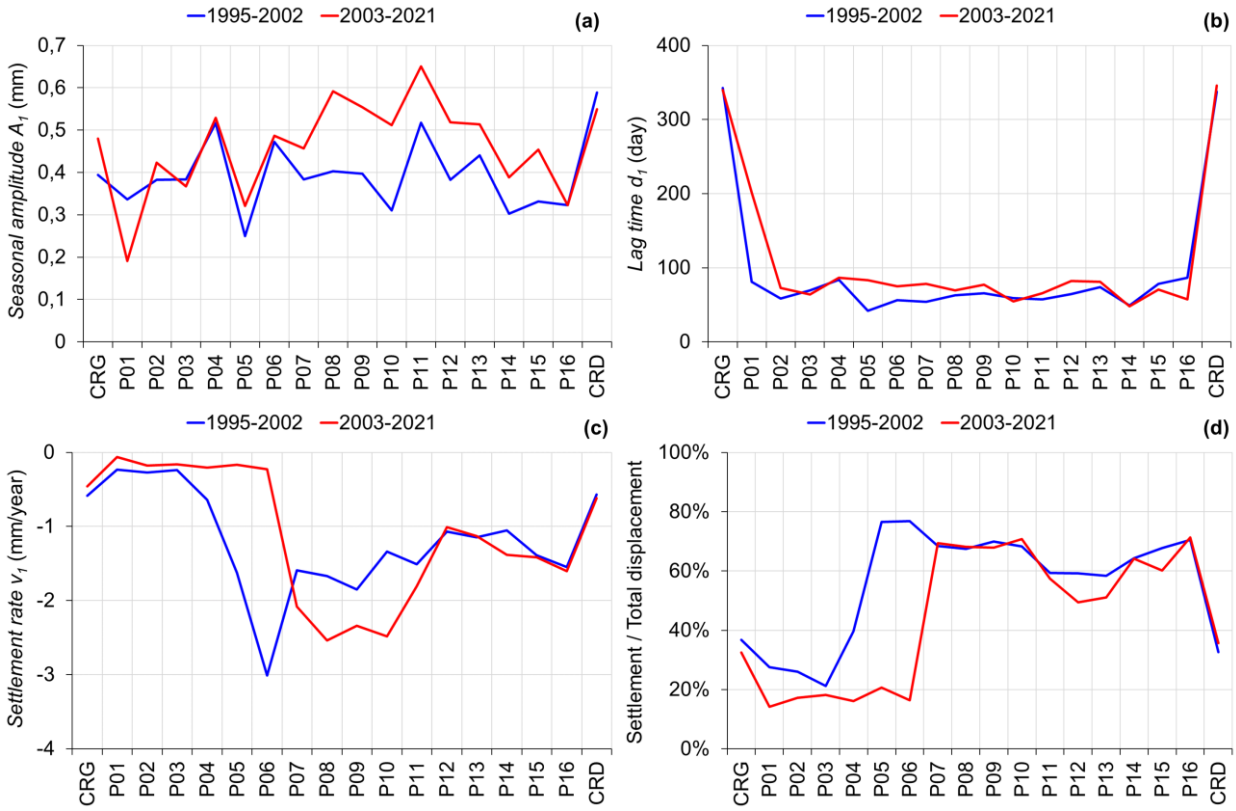

Figure 10. Results of the HST analysis for the whole bridge on two intervals before (1992-95) and after (2003-21) reinforcement for P05 and P06 – after reinforcement for P01 to P04, and before reinforcement for CRG, CRD, and P07 to P16: (a) Amplitude of seasonal reversible effects A_1, (b) Lag time d_1, (c) Settlement rate v_1, and (d) Settlement / Total displacement ratio.

Both HST and BDLM models have been used to indentify the contributions of reversible effects, which are seasonal variations due to external temperature, hydrostatic effects due to tide variations (buyoyancy), and irreversible effects (ageing, creep) on settlement measurement. Examples of application are given in Figures 7 and 8 for P02 in 2003-21 (after reinforcement) and P14 in 2003-21 (without reinforcement). Results obtained for all 18 instruments are reported in Figure 10. Before reinforcement, it has been demonstrated (Valdeyron, 2023) that:

- Seasonal effects, considered as reversible effects, are fitted with a twelve-month period of sinusoidal function, all piers are synchronous, and abutments are in opposite phases. Amplitudes of variations are all between 0.3-0.5 mm;
- The contribution of the tide effects on displacement is not significant and settlements due to water level variation (buoyancy) are reversible;
- 99% of the settlement is explained by the model which doesn't need more information to model the bridge's behavior;
- As a consequence, that entails that the tramway traffic has insignificant influence on settlement;
- The settlement rate is assessed to be 1-3 mm/year before reinforcement.

After reinforcement, it has also been demonstrated (Valdeyron, 2023):

- Amplitudes of seasonal effects (outdoor temperature) and their phase shifts are not affected by reinforcement;
- Before reinforcement, creep settlements were represented at about 60 to 80% of the total settlements (including seasonal effects); after reinforcement, this ratio was reduced to less than 20% (knowing that settlements are stabilized with a velocity $v_l \leq 0{,}2$ mm/year).

Effects of Micropile Reinforcements on Tilting

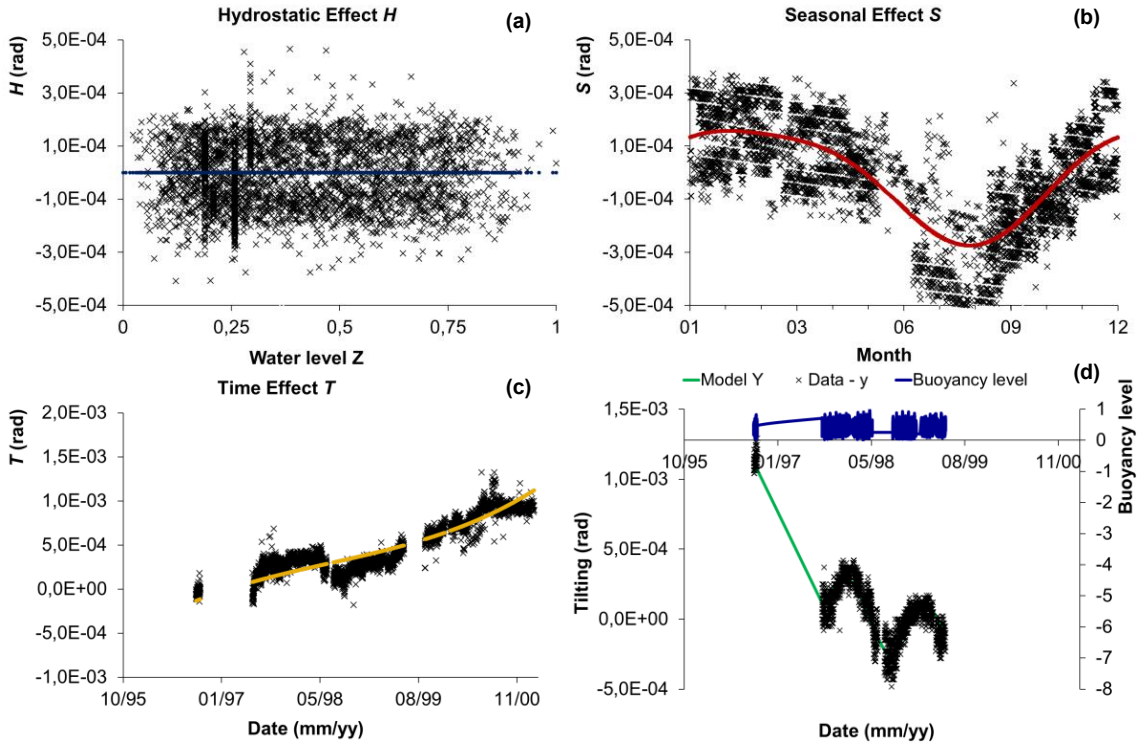

Figure 11. Results of the HST analysis of P05 measurements in 1992-2002 (before reinforcement): (a) Hydrostatic effect H, (b) Seasonal effect S, (c) Time effect T, and (d) Data, model and buoyancy level.

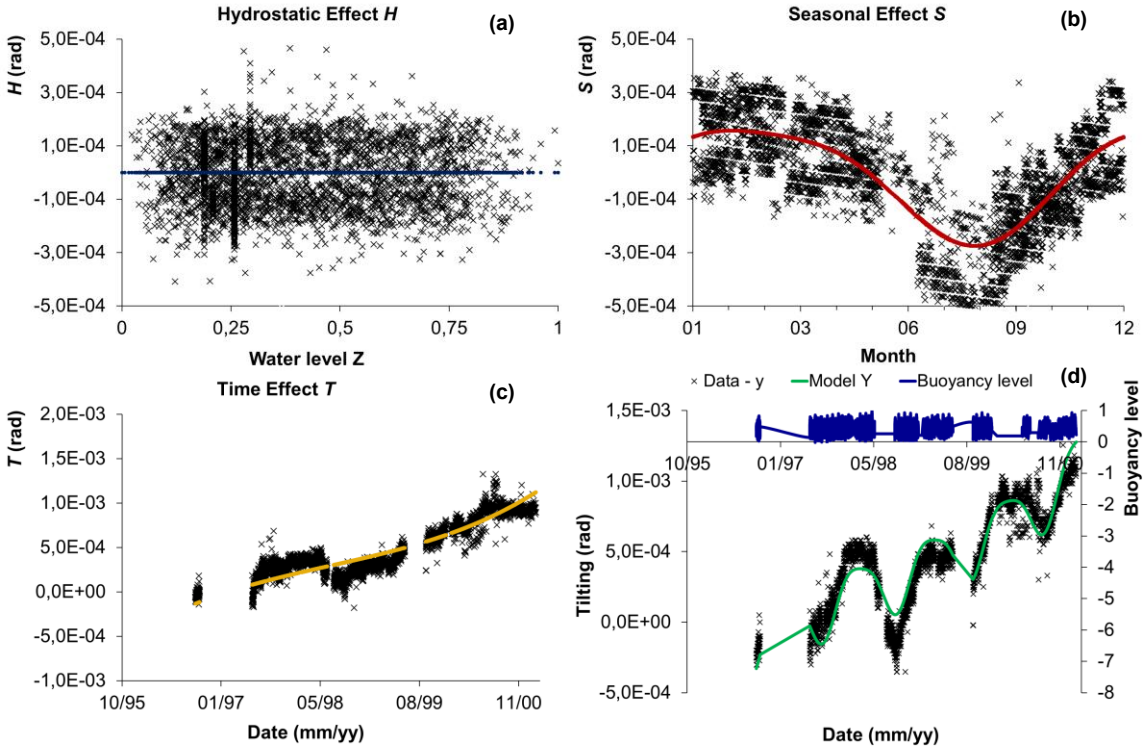

Figure 12. Results of the HST analysis of P06 measurements in 1992-2002 (before reinforcement): (a) Hydrostatic effect H, (b) Seasonal effect S, (c) Time effect T, and (d) Data, model and buoyancy level.

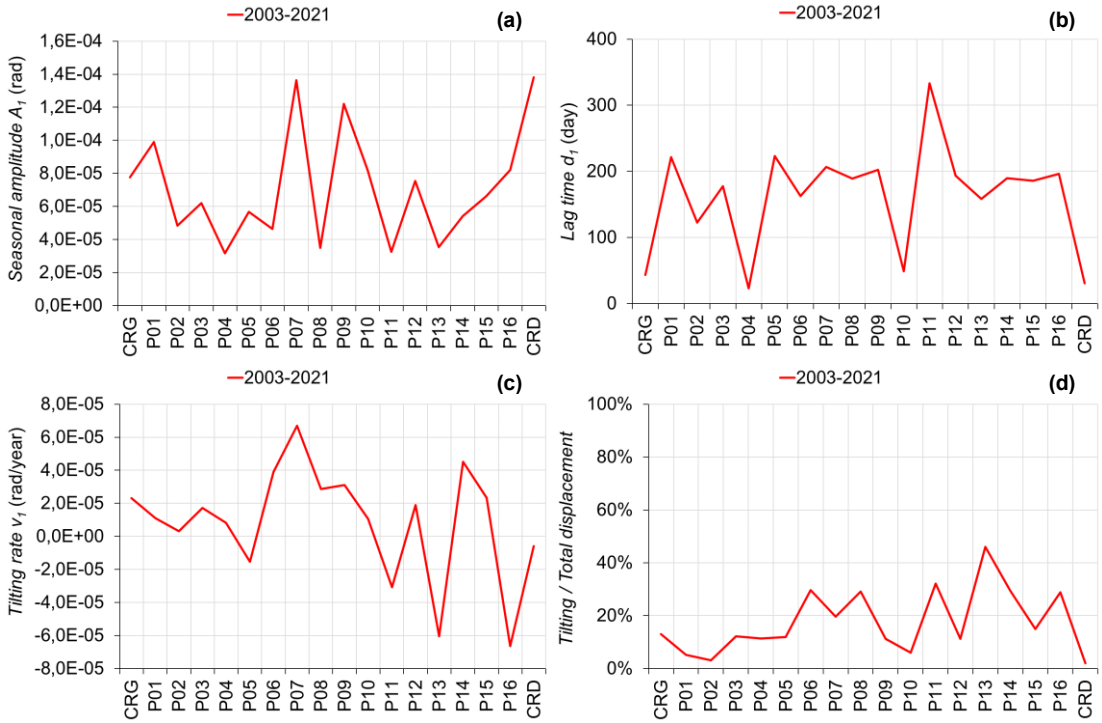

Figure 13. Results of the HST analysis of tiltmetrer measurements for the whole bridge in 2003-21 (before reinforcement for CRG, CRD, and P07 to P16; after reinforcement for P01 to P06: (a) Amplitude of seasonal effects A_1, (b) Lag time d_1, (c) Settlement rate v_1, and (d) Settlement / Total displacement ratio).

Analysis was carried out on tilting measurements. For all 18 instruments, obtained results are shown in Figure 13. Two periods are explored:

- 1996-2002: this period corresponds to the unreinforced configuration for P05 and P06 (Figures 11 and 12);
- 2003-2021: this period is also an unreinforced configuration for P07 to P16 and the abutments, and a reinforced configuration for P01 to P06 (Figure 13).

Tilting measures, given in radians, are positive in the downstream direction and negative in the upstream one. The downstream direction correlates to North/North-West, the upstream direction correlates to South/South-East (S/S-E). To be consistent, sign convention is choosen as follows: tilting rate v_1 (rad/year) is positive when tilting is oriented toward the downstream direction, and negative on the upstream direction.

As a whole, the structure is tilting downstream (in a positive direction), except for P11, P13, and P16, which is consistent with the analyses reported in the 2013 diagnostic report on the sub-fluvial slopes (Artélia & Levillain, 2013), which noted that, overall, the sub-fluvial slopes were subsiding more markedly downstream than upstream.

Before reinforcement, P05 and P06 were tilting irreversibly (T effect) in opposite directions, respectively in the upstream direction and downstream direction, with a tilting rate of about $1.5\text{-}2.0 \cdot 10^{-4}$ rad/year. Seasonal effects (outdoor temperature) lead to negative (upstream or North-facing) tilting of piers. Hydrostatic effects are due to current reversal during slack tide. The HST model is able to explain 69% to 98% of the measurements. The proportion of seasonal effects on tilting is variable (3% to 39% for all piers, except for P01 and P02, and hydrostatic effects (buyoancy due to tide cycles) explain less than 0.3% of overall tilting—mainly due to ageing (50% to 97%). Notable exceptions are P01 and P02, which, after reinforcement, are mainly influenced by outdoor temperatures (46% to 47%).

For P01 to P06, effects of reinforcements on tilting rate reduction are illustrated in Figure 12: for reinforced piers, the absolute value of tilting rate is less than $2.0 \cdot 10^{-5}$ rad/year, whereas before reinforcement this rate was 10 times higher. Irreversible tilt represents 20-45% of overall tilting before reinforcement, a value which is reduced to 12% after reinforcement.

Effects of Reinforcements on Thermal Behaviour

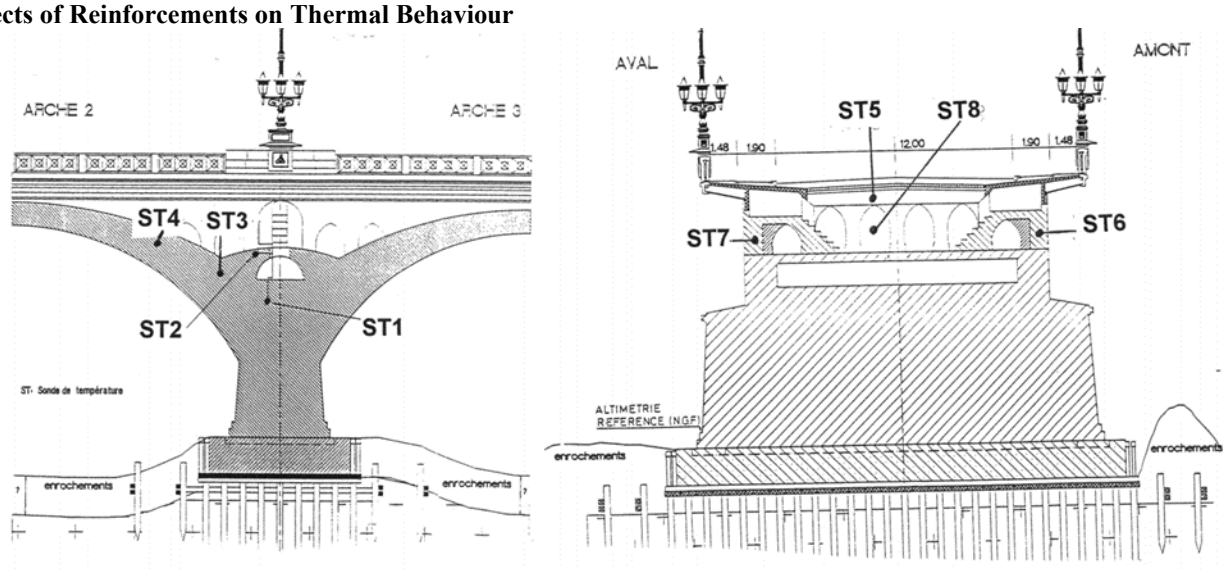

Figure 14. Temperature sensors layout.

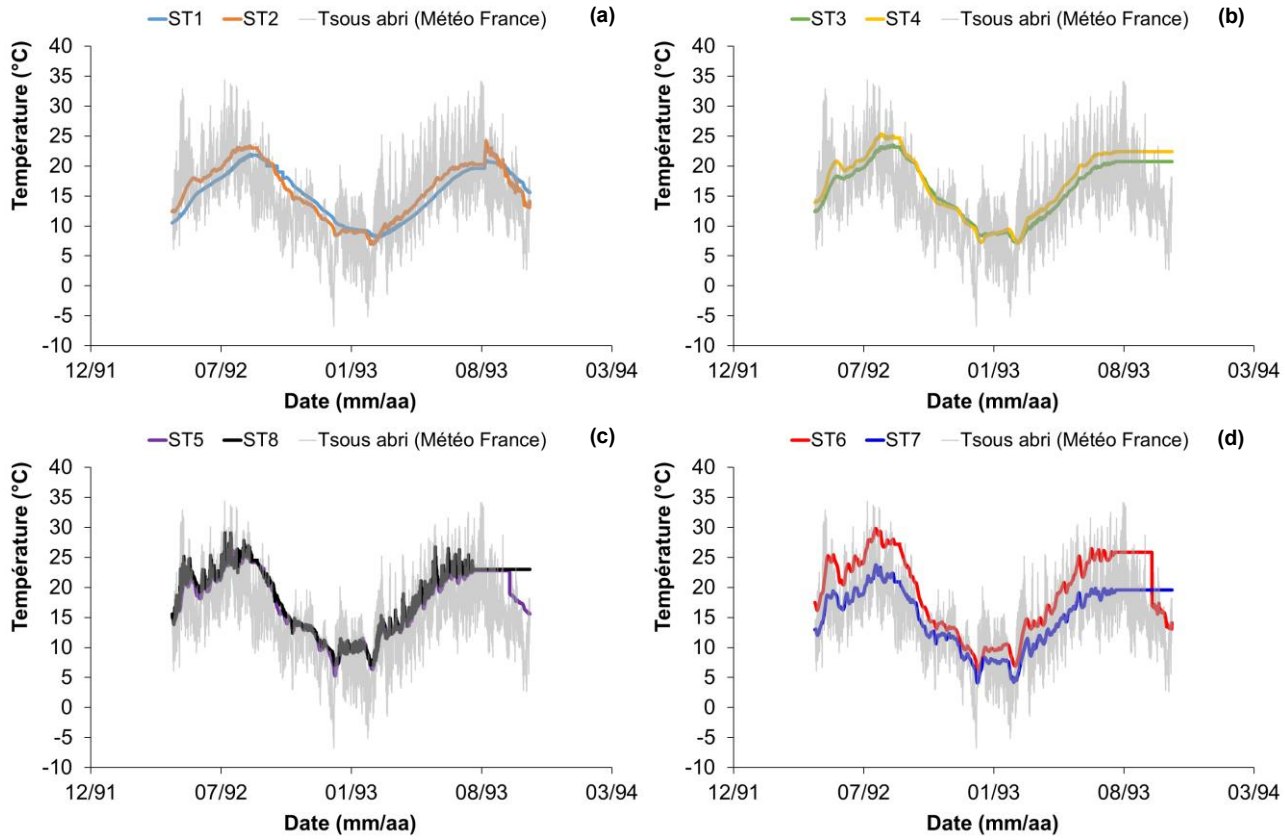

Figure 15. Temperature measurements in 1992-93: (a) Temperature of the masonry of the pier, (b) Temperature of the vault, (c) Temperature of the deck and temperature inside the spandrels, and (d) Temperature on the spandrels.

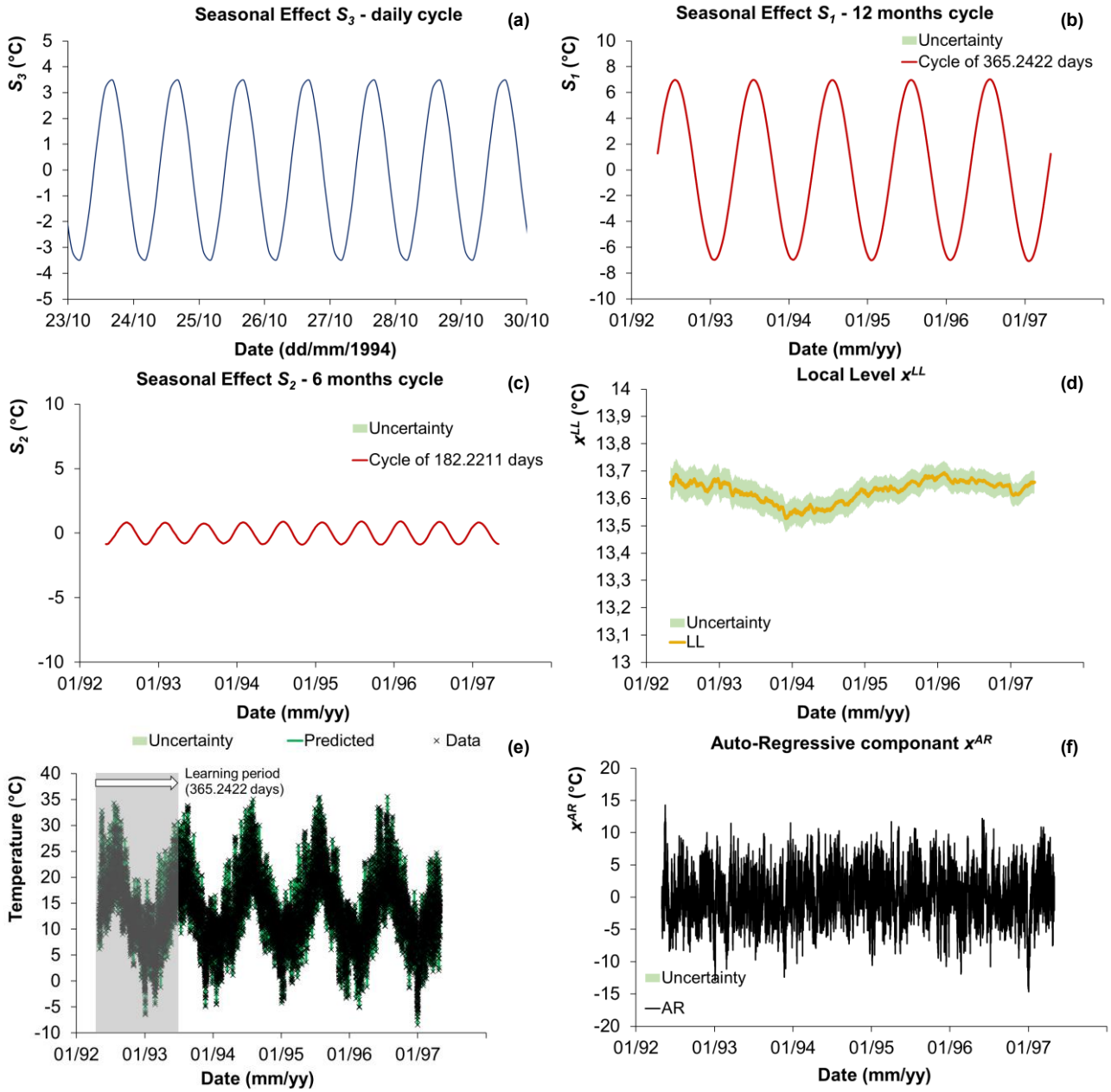

Figure 16. Analysis of meteorological data with OpenBDLM in 1992-97: (a) Daily effect S_3, (b) Seasonal effect 364.2422 days cycle S_1, (c) Seasonal effect 182.2211 days cycle S_2, (d) Local Level x^{LL}, (e) Datas and model, and (f) Auto-Regressive x^{AR} component.

As mentioned, the design and the works carried out could result in a complex behavior between an arch bridge and a box girder bridge. An analysis of the thermal behavior of the bridge can provide valuable information. The thermal behavior of a box girder bridge is characterized by the absence of deformations on the spans and the concentration of these on the abutments.

The seasonal effects on settlements analysis shows that settlements are increasing during the warm season: the thermal expansion of the arches (when the arch length increases) leads to an increase in measured settlements. For all piers, the peak value of settlements is obtained in September/October with a two-month time lag in the summer season (July/August) that is explained (see further) by the thermal inertia of the masonry structure. This confirms that the behavior of the structure is typical of a masonry vault. On the abutments, the behavior is different: thermal expansion leads to a local rise in the structure,

reflecting edge effects (e.g., prevented movements). For abutments, seasonal effects on tilting measurements are explained as follows: the abutments are massive sections of masonry which act like gravity dams by tilting in the North-facing (colder) direction during the summer.

The behavior of arches is more complicated to analyze: due to the vertical gradient between intrados and extrados, the vault rises during summer, but this heightening depends on the horizontal gradient between the South (warmer) face and North (colder) face, so the rising should be more significant on the South face than North face. Thus, the thermal deformations cause the arch to twist and the pier to tilt toward the upstream (South) direction. On the other hand, in the summer, when the pier tends to tilt downstream, the arches tend to tilt it upstream.

Pier 1 and Arch 2 (between P01 and P02) were thermally monitored between May 1992 and October 1993 with the installation of eight temperature sensors, arranged according to the layout shown in Figure 12. The aim of Temperature Sensors 1 to 8 was to determine temperature changes and gradients in the structure between:

- Upstream (South) and downstream (North);
- The lower and upper surfaces; and
- The inside and outside of the structure.

All the data is shown in Figure 15. An analysis using a Bayesian model (OpenBDLM) was carried out in 1992-97 on the basis of meteorological data (sub-shelter temperature, Météo-France data given every three hours at the Mérignac Station a few kilometers from the bridge). The results are shown in Figure 16.

The conclusions that can be drawn from the analysis are:

- The temperatures in the less massive sections (Spandrels ST6 and ST7, Deck ST5, and the Internal Arches Rooms ST8, as seen in Figure 15 c and d) generally follow daily variations and have no seasonal phase shift;
- The temperatures of the more massive sections (masonry of the piers and the vaults - see Figure 15 a and b) are little influenced by daily variations and show a phase shift with annual seasonal variations of around 41 days for ST1 (body of the masonry) and around 35 days for ST2, ST3, and ST4 (vault);

The structure is therefore subject to gradients:

- Upstream/downstream on the vaulted piers and spandrels, which can explain the downstream tilting (i.e., to the North, on the cold side) during the summer period (when the gradient is at its maximum) of the abutments that can be considered as weight dams;
- Extrados/intrados on the vaults, which lead to a rotation of the normal fiber-neutral sections at the ends of the vaults, which may explain the seasonal effects on the tilting of the piers;
- Deck/foundations on the piers, where the pier bases, in contact with the water, have a lower temperature in the summer and a higher temperature in the winter than the deck.

The temperature gradient between the annual seasonal effects S_1 and the arch (ST3 and ST4) is of the order of +6°C in the summer and -2°C in the winter (Figure 17e). The difference is greatest in September and May, which corresponds to the seasonal effects on settlement in 2003-2021 (see Figure 8b):

- Settlement is greatest in September and October, when thermal expansion of the arch is at its maximum. It should be noted that at this period, the temperature in the internal arches rooms, still relatively close to its peak, leads to thermal expansion of the pillars and consequently to the loading of the vault, which accentuates the phenomenon;
- Settlement is minimal in March and April, when the thermal expansion of the vault is close to its minimum; at this time the internal pillars (in arches rooms) are still contracted, which means that the load on the vault is lighter;

The temperature gradient between the annual seasonal effects S_1 (temperature under shelter corrected for daily variations) and the masonry body (ST1) of the pier is of the order of +5°C in the winter and -4°C in the summer (Figure 17a). The difference is greatest in mid-November and mid-May.

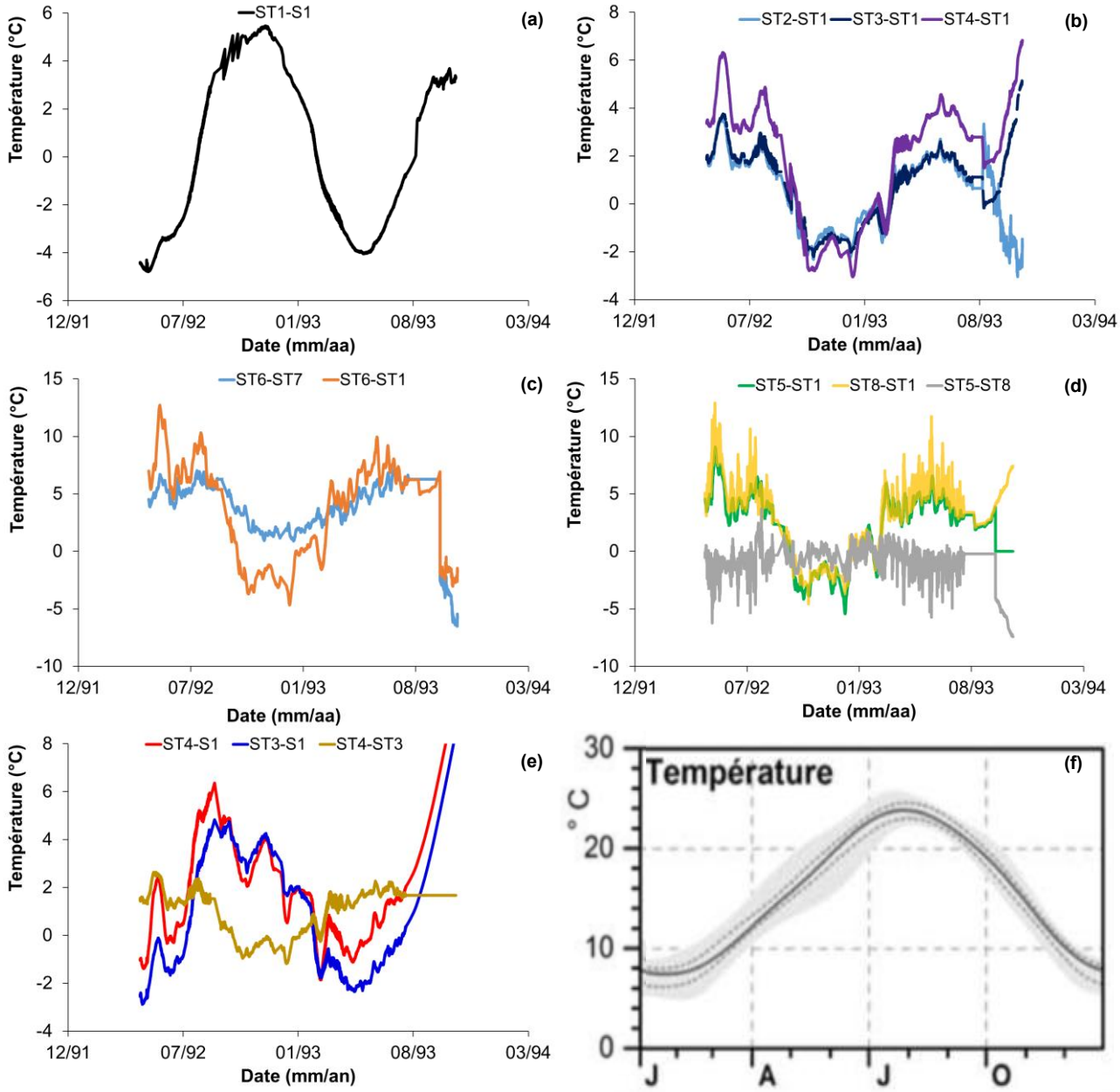

Figure 17. Temperature data on the structure in terms of temperature difference between: (a) pier masonry and annual seasonal effects, (b) vault and pier masonry, (c) pier and spandrels North- and South-facing sides of the spandrels, (d) pier and deck and internal arches rooms, (e) vault and annual seasonal effects, and (f) temperature of the water of the Garonne, at the surface, in Bordeaux (source: MAGEST, 2006-2016).

Effects of Thermal Behavior on Reinforcements

The method was also applied to the stress gauges located in micropiles, and results for P01 to P06 are consistent with the settlement analysis. It is confirmed that seasonal effects are in opposite phase with load on micropiles: load transfer is maximized in warmer periods (September / October) when settlements (in absolute values) are also at their peak values, and minimized in cooler periods (March / April), as llustrated in Figure 18.

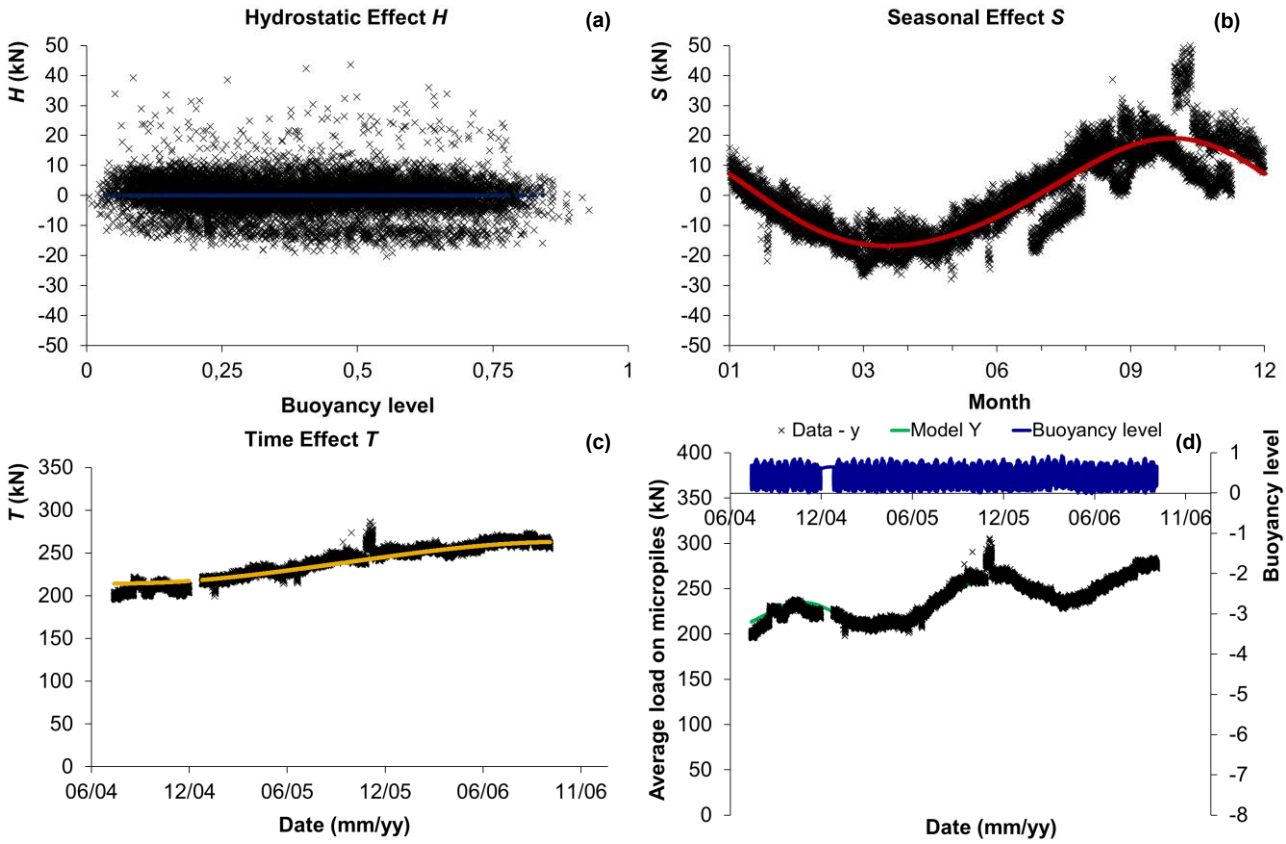

Figure 18. Results of HST analysis of P01 measurements in 2004-06 (after reinforcement): (a) Hydrostatic effect H, (b) Seasonal effect S, (c) Time effect T, and (d) Data, model and buoyancy level.

RESULTS OF THE ANALYSIS OF THE CORRELATION OF TEMPERATURE AND TIDE WITH SETTLEMENTS

A three-time series BDLM model is built including settlement measurements of P06, outdoor temperature, and tide level in order to correlate settlement variations of the pier with tide and temperature evolutions. To do that:

- Settlement series are modeled with two components: a Local Level (*LL*) and an Autoregressive (*AR*);
- Temperature is modeled with four components: a Local Level (*LL*), two periodic components (T = 365.24 days and T = 1 day) and an Autoregressive (*AR*) component;
- Tide is considered as an explicative variable and modeled with two components: a Local Level (*LL*) and an Autoregressive (*AR*) component. Tide level measures are considered as exact (no error) on the model, which is achieved by using an observation variance tending to zero and a model error variance of the order of magnitude of the tidal range (as explained in Goulet, 2017).

The learning period (testing datas) is reduced to the 180 first days. The model's ability to predict settlement trends as a function of variations in outside temperature and tidal level has been demonstrated (Figures 19 to 21). The regression coefficient obtained between the settlement measurements and the temperature is negative, which confirms that they vary in opposite directions: when the temperature is at its highest, settlement is at its lowest, and vice versa. For tidal measurements, the regression coefficient is positive (same direction) which is consistent with previous analysis: at high tide, settlement is at its superior peak (reduced settlement) due to the buoyancy effect. The ratio between these coefficients indicates that the effect

of temperature on settlement is 8 times higher than the tide influence. In practice, it is therefore possible to simulate the effect of extreme variations in temperature or tide (e.g., a flood).

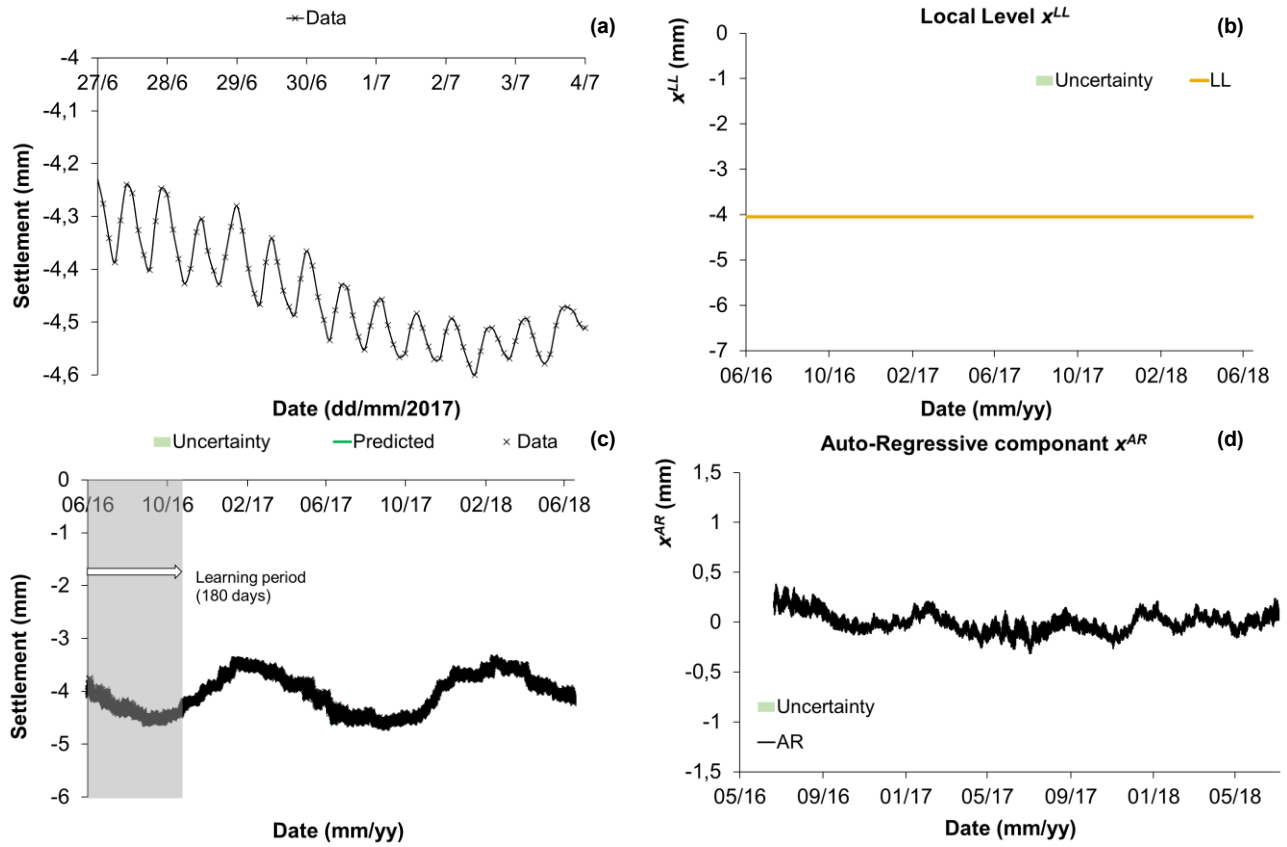

Figure 19. Results of OpenBDLM analysis of P06 measurements in 2016-18 (after reinforcement): (a) One week of measurements, (b) Local level, (c) Data and model, and (d) Autoregressive component.

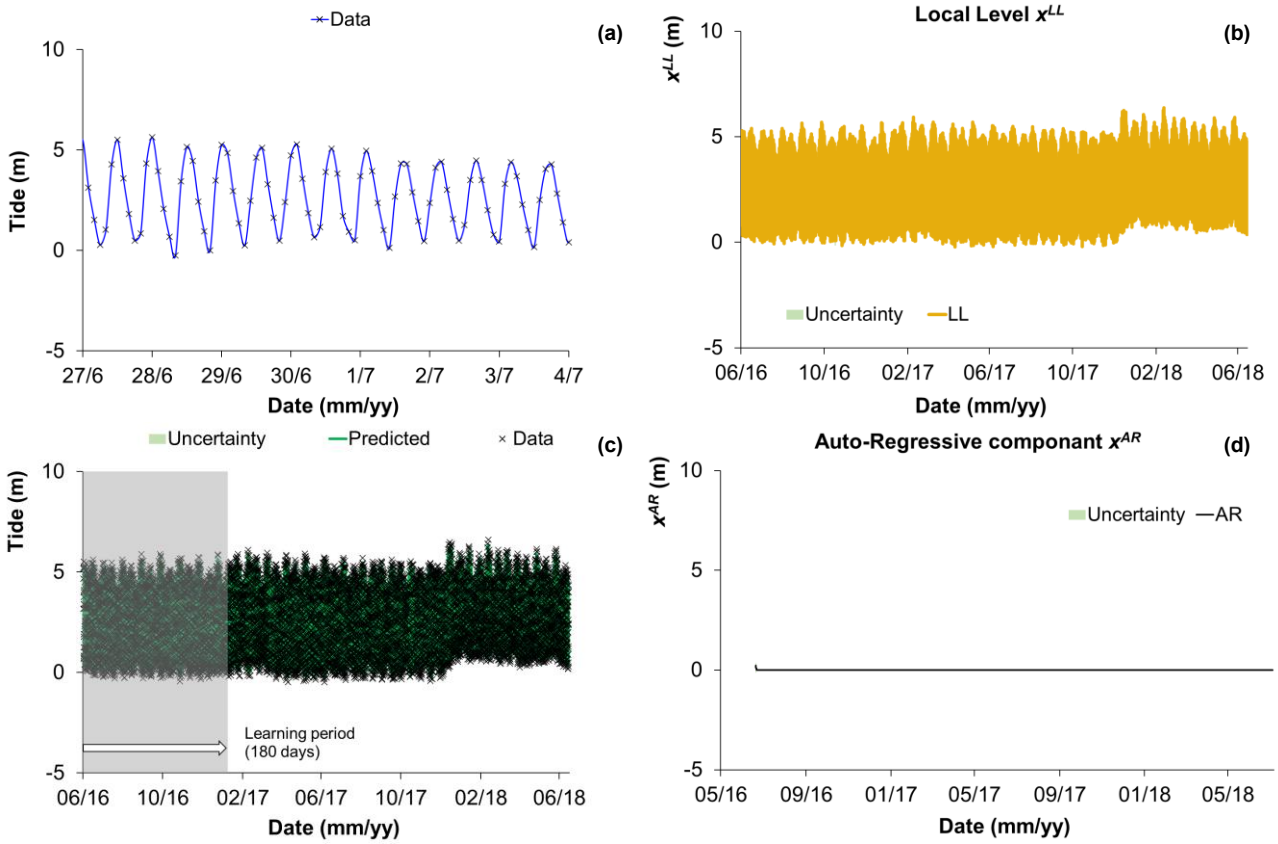

Figure 20. Results of OpenBDLM analysis of tide measurements in 2016-18: (a) One week of measurements, (b) Local level, (c) Data and model, and (d) Autoregressive component.

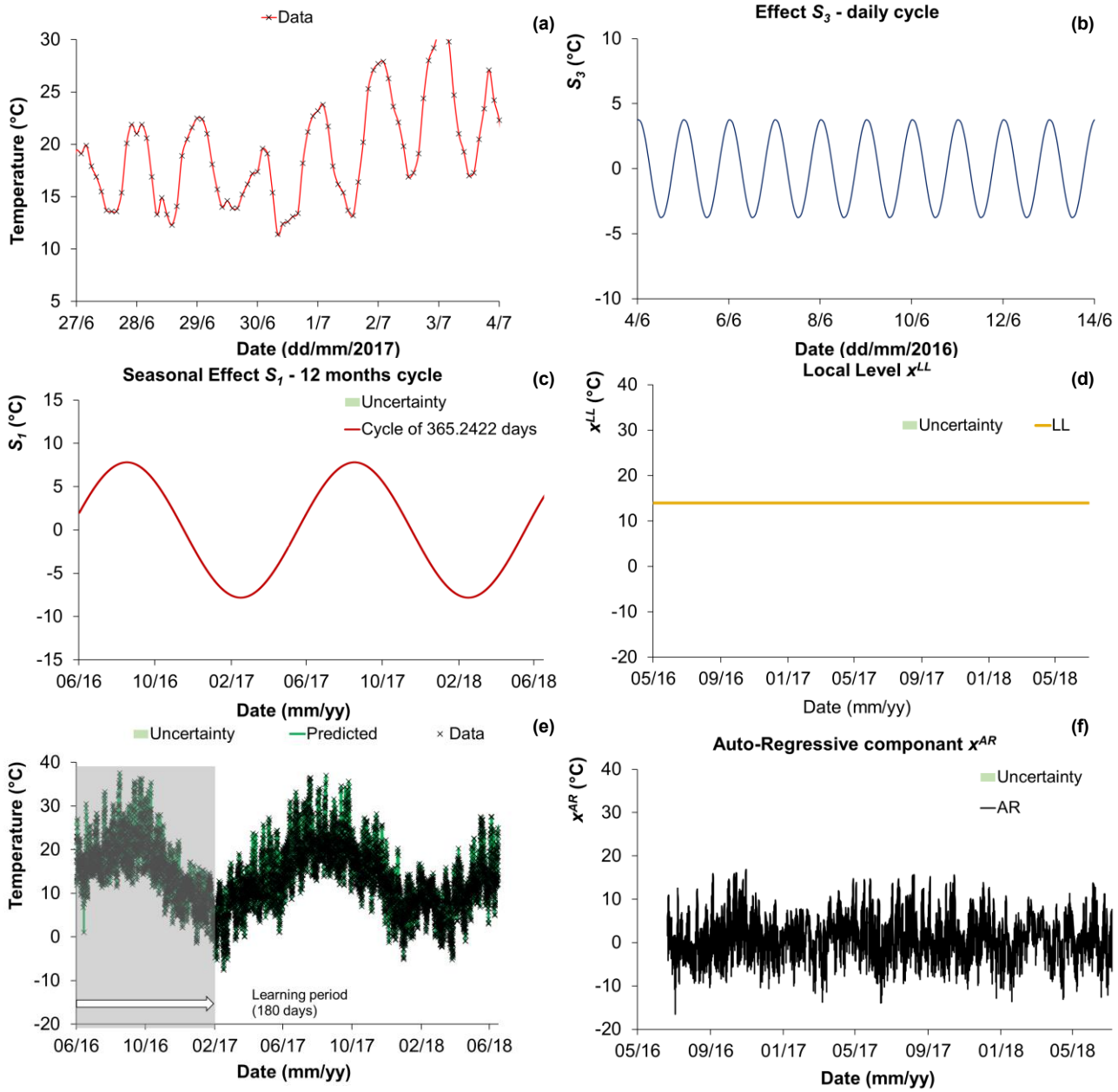

Figure 21. Results of OpenBDLM analysis of outdoor temperature measurements in 2016-18: (a) One week of measurements, (b) Daily cycle, (c) 365.2422 days cycle, (d) Local level, (e) Data and model, and (f) Autoregressive component.

RESULTS OF THE DETECTION OF ANOMALIES ANALYSIS

An advantage of BDLM compared to HST consists on its capacity to detect anomalies in the structure's behavior. This is done by considering a set of two models: model (M_1) is used to modelize the normal behavior of the structure, and the second model (M_2) is used to handle abnormal behavior. As seen in our case, the M_1 model is composed of a Local Trend (LT) component to handle the ageing of the structure, three periodic components to assess seasonal effects (S_1 = 365.24 days and S_2 = 182.22 days) and tide effects (S_3 = 1 day), and an autoregressive component to evaluate what is not caught by the model. The second model, M2, defined in order to model abnormal behavior, is composed of the same components, except for LT which is substituted by a Local Acceleration (LA) component to represent settlement rate variations during works. The

analysis is applied on P07, P08, and P09 in order to explore dependancies between the piers' behavior and works realized on it and influences of a pier settlement on its neighbors.

Settlement Measure Analysis

Each of the settlement anomalies detected between May and June 2021 (see Figures 22 to 25) are attributed to the geotechnical investigations (destructive core drilling followed by pressuremeter tests carried out through the pier and its foundation) that occurred during this period. Detection is quite accurate: for P07, geotechnical investigation began on 22 April 2021 and acceleration of settlements due to boreholes drilled within the foundation of this pier was detected on 5 May with a probablity of 100% (Figure 22a). For P09, the anomaly was detected on 4 May with a probability greater than 74% when investigations began on 22 April. Before and after investigations, settlement rates increased from 1.6 mm/year to 2.8 mm/year for P07 (see Figure 22c), from 2.3 mm/year to 4 mm/year for P08 (see Figure 23c), and from 1.5 mm/year to 2.6 mm/year for P09 (see Figure 24c).

This confirms the sensitivity of the structure to external sollicitations, especially on the foundations. In addition, positive effects, such as benefits or rip-rap works realized in 2016-18 and illustrated in Figure 24c, could have been highlighted. For example, settlement rates were reduced from 2.07 mm/year to 1.6 mm/year for P07, and from 2.3 mm/year to 1.5 mm/year for P09. Excessive settlements and acceleration of these by driven dophins works executed in 2004 are also detected for P09 and P08 (Figures 23c and 24c); for the latter, the settlement rate is multiplied by a factor of 2 (1.4 to 3 mm/year). P07 is not affected by driven dolphin works, confirming that, assuming relatively controlled settlement, P07 is independent of its neighboring piers. Lastly, the consequences associated with the installation of the two test micropiles drilled through the masonry and foundations of P08 are also detected, with a very significant acceleration in settlement during drilling and the attainment of a settlement rate of around 18 mm/year. This rate was reduced after the micropiles were sealed to the masonry (14 September 2022), but was still significant (10 mm/year) in March 2023, which suggests that settlement had not yet stabilized (see Figure 23c). As the model can forecast the normal behavior of P08 (Figure 25), it is possible to accurately determine irreversible settlements due to the first micropile (from August 4-18) and the second micropile (from August 18-25) and since the sealing of these to the masonry (14th of September). It was then possible to identify the critical phases that led to significant settlement and, as a result, to set the execution methods for future work on P07 to P16.

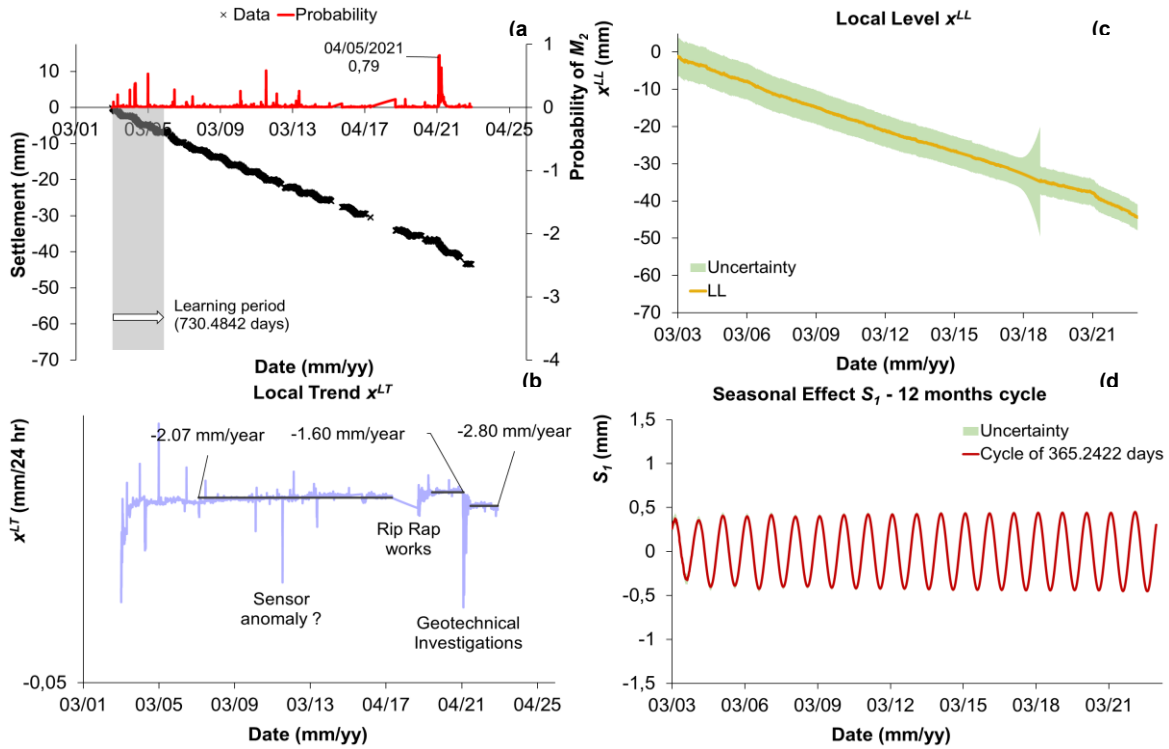

Figure 22. Results of OpenBDLM analysis of P07 measurements in 2003-23: (a) Data and probability of abnormal Model M_2, (b) Local level x^{LL}, (c) Local trend x^{LT}, and (d) 364.2422 days cycle S_1.

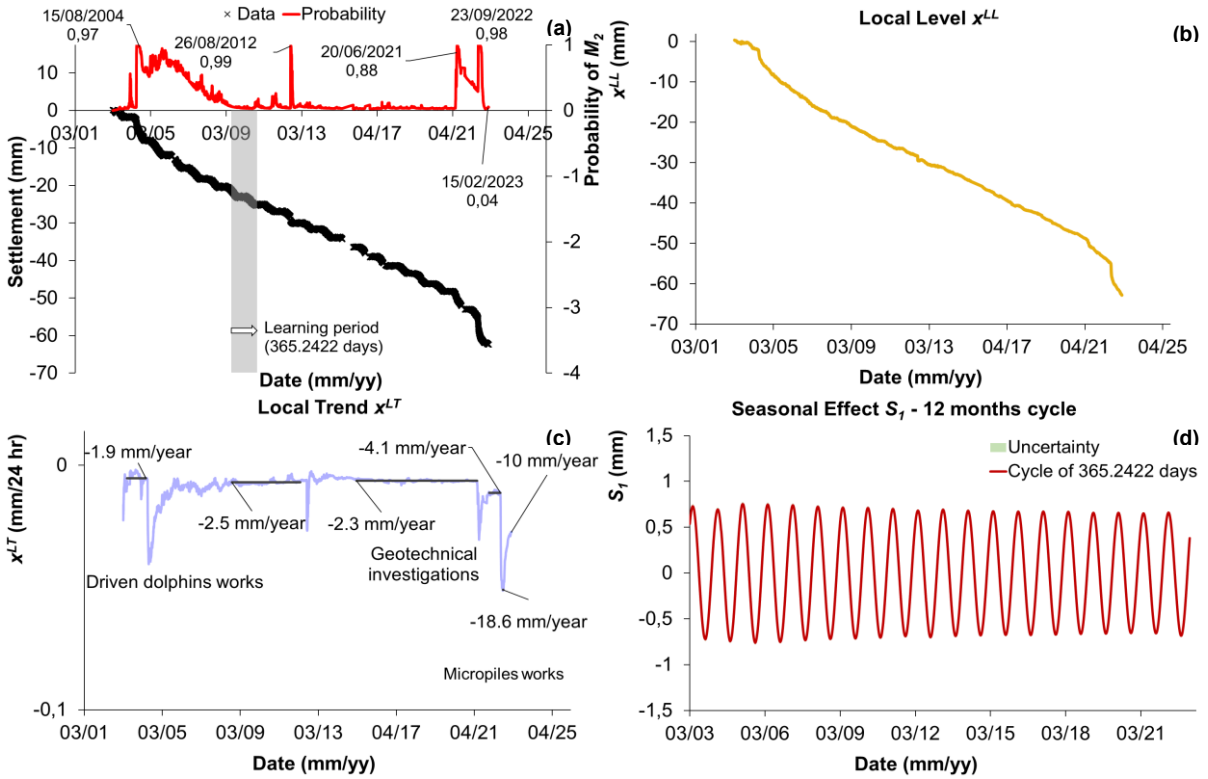

Figure 23. Results of OpenBDLM analysis of P08 measurements in 2003-23: (a) Data and probability of abnormal Model M_2, (b) Local level x^{LL}, (c) Local trend x^{LT}, and (d) 364.2422 days cycle S_1.

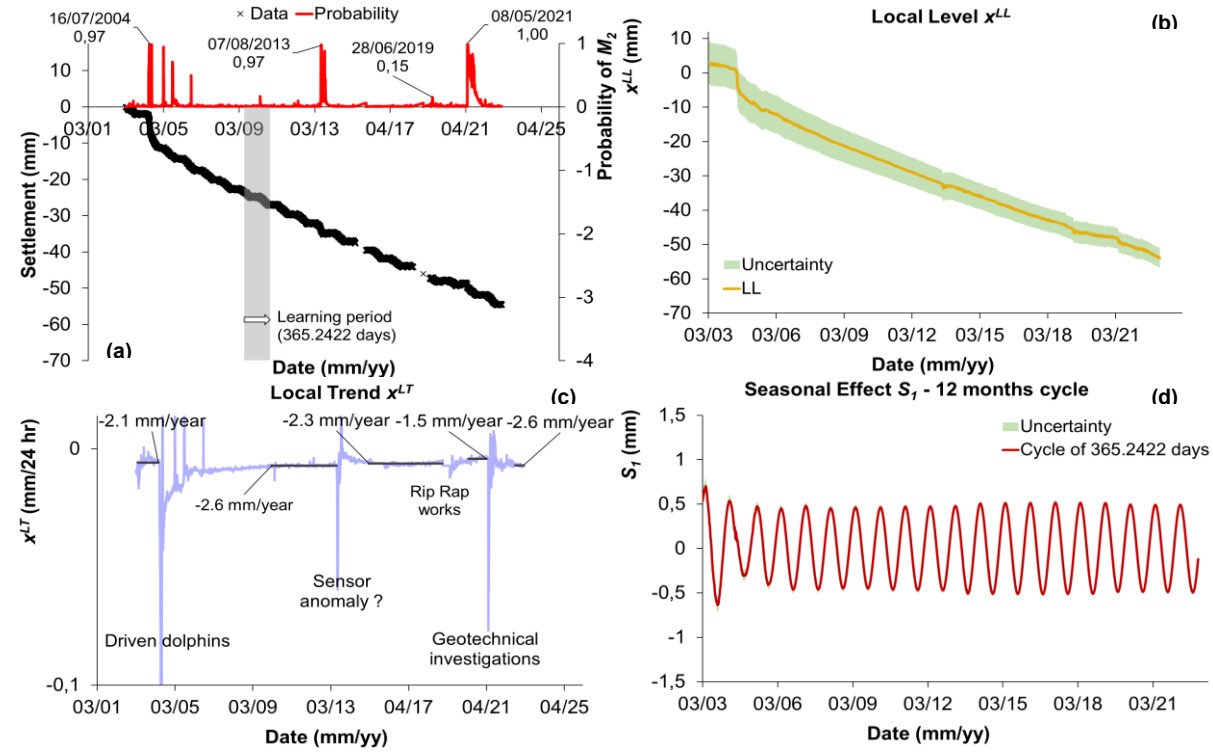

Figure 24. Results of OpenBDLM analysis of P09 measurements in 2003-23: (a) Data and probability of abnormal Model M_2, (b) Local level x^{LL}, (c) Local trend x^{LT}, and (d) 364.2422 days cycle S_1.

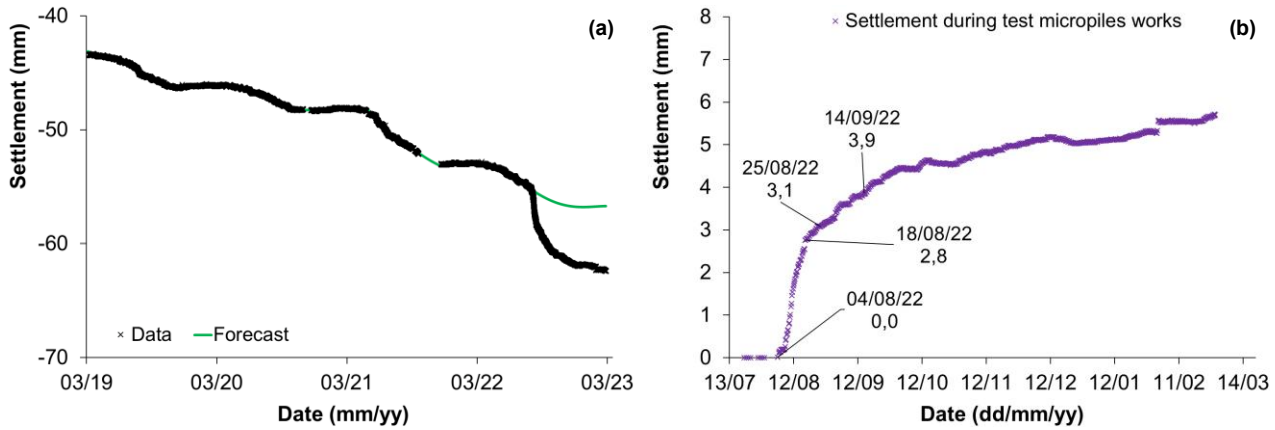

Figure 25. Results of OpenBDLM analysis of P08 measurements during test micropiles works: (a) Data and forecast settlements, and (b) Settlements due to works.

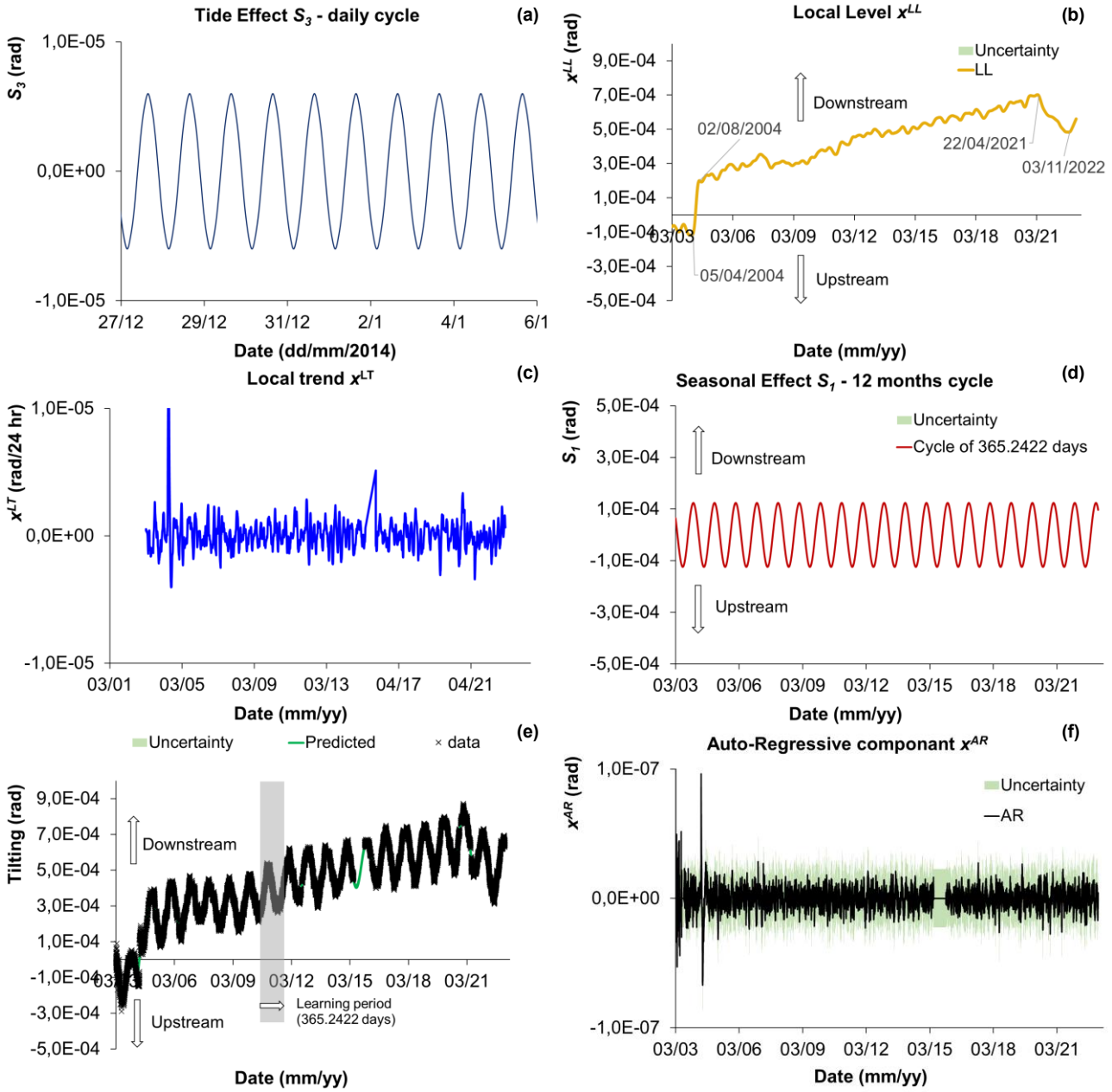

Figure 26. Results of OpenBDLM analysis of P09 measurements in 2003-23: (a) Daily cycle, (b) 364.2422 days cycle S_1, (c) Local trend x^{LT}, (d) Local level x^{LL}, (e) Data and model, and (f) Autoregressive component (AR).

Tilting Measure Analysis

The model is then applied to the analysis of inclinometric measurements of the structure. For P09, the results show seasonal cycles (due to the outside temperature) and daily cycles (due to the reverse of the tide), with an order of magnitude difference between the amplitude linked to thermal movements (Figure 26) and those linked to the tide. The start and end of the driven dolphin works have also been identified, marking a downstream tilting of the pier. The impact of the geotechnical surveys carried out in April/July 2021 was also observed, with the pier tilting upstream, which is consistent with the fact that the investigations were carried out on the upstream side of the bridge. This tilting seems to be stabilized since the end of 2022, with a tendency toward a downstream tilting. All results are not reported here but similar observations can be made for the

other piers. The model is able to detect changes in the tilting local level of P09 on 22 April 2021, the day of the beginning of geotechnical investigations (see Figure 26d).

CONCLUSION

Sensitive structures such as the Pont de Pierre require appropriate tools to analyze monitoring data and provide convincing explanations of the structure's behavior. Both methods explored (HST and BDLM) provide consistent results. In this way, it was possible to quantify the relative contributions of external effects (temperature, tidal height, and consequences of work on the structure).

The two models give comparable results, and provide a basis for understanding the behavior of the structure, particularly its thermal behavior. The theoretical behavior of the Pont de Pierre, given its characteristics, could fall somewhere between a caisson bridge and a masonry vault. The analysis carried out confirmed that the bridge would function as a vault, and highlighted singularities at the abutments and P10.

It was possible to identify and quantify the effects of the works on the structure in terms of tilting of piers and settlement: accelerations were observed during the works and stabilization after the micropiles had been installed. This opens up the prospect of being able to detect any anomalies in the behavior of the structure as soon as possible during future work.

Finally, another application could be to simulate the effects of extreme temperatures or water levels (flooding) in the context of global climate change in order to evaluate these effects on the structure.

REFERENCES

Artélia & Levillain, J.-P. (2013). Etudes et suivi des travaux de réparation de la protection des talus sous-fluviaux et des pieds des piles - Rapport de diagnostic complémentaire - AVP des travaux de restauration, Artélia, Paris, France.

Bonelli, S. (2008). "On pore-pressure analysis in earthdams." *International Water Power and Dam Construction,* 60(12), 36-39.

Bonelli, S. (2009). "Approximate solution to the diffusion equation and its application to seepage-related problems." *Applied Mathematical Modelling*, 33(1), 110-126.

Carrère, A., Colson M., Goguel B., Noret C. (2000). "Modelling: a means of assisting interpretation of readings." *Proc., 20th Int. Congr. on Large Dams* , ICOLD, Beijing, China, 1005-1037.

Ferry, S., Willm G. (1958). "Méthodes d'analyse et de surveillance des déplacements observés par le moyen de pendules dans les barrages." *Proc., 6th Int. Congr. on Large Dams*, ICOLD, New York, USA, 1179-1200.

Forbes, J.D. (1846). "Account of some experiments on the temperature of the earth at different depths and in different soils near Edinburgh." *Transactions of The Royal Society of Edinburgh,* 16, 189-236.

Gaudot, I., Nguyen, L.H., Khazaeli, S., and Goulet, J.-A. (2019). "OpenBDLM, an Open-Source Software for Structural Health Monitoring using Bayesian Dynamic Linear Models." *Proc., 13th Int. Conf. on Applications of Statistics and Probability in Civil Engineering (ICASP13)*, Seoul, South Korea.

Goulet, J.-A. (2017). "Bayesian Dynamic Linear Model for Structural Health Monitoring." *Struct. Control and Health Monit.*, 24.

Goulet, J.-A, Koo, K. (2018). "Empirical validation of Bayesian Dynamic Linear Model in the context of Structural Health Monitoring." *Journal of Bridge Monitoring*, 23.

Guedes, Q.M., Coelho, P.S.M. (1985). "Statistical behaviour model of dams." *Proc., 15th Int. Congr. on Large Dams, Lausanne*, ICOLD, Lausanne, Switzerland, 319-334.

Valdeyron, G., Losset, P., Dubroca, S., Mariko, M. (2023). "Assessment of Pont de Pierre settlements by Bayesian Dynamic Linear Model (BDLM) – Comparison with Hydrostatic-Season-Time (HST) model and benefits for the Pont de Pierre reinforcement works monitoring." *Proc., 9th Int. Congr. on Environmental Geotechnics (9ICEG)*, Paris, France.

Young, P. (1998). "Data-based mechanistic modelling of environmental, ecological, economic and engineering systems." *Environmental Modelling & Software*, 13,105-122.

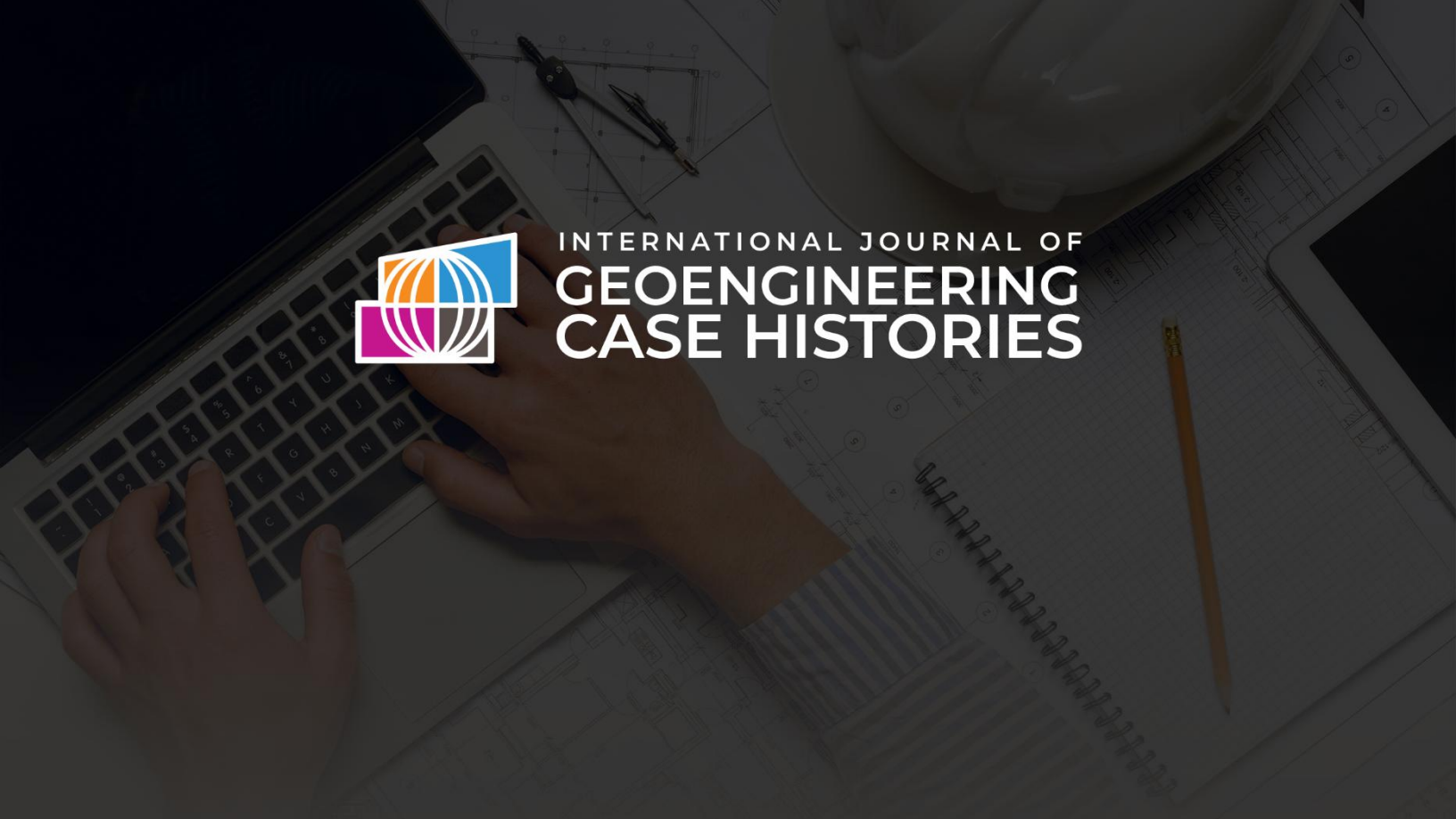

INTERNATIONAL JOURNAL OF
GEOENGINEERING
CASE HISTORIES

The Journal's Open Access Mission is generously supported by the following Organizations:

dar
a Sidara company

Geosyntec consultants
engineers | scientists | innovators

ConeTec
MUD BAY DRILLING
LANKELMA
Geotech DRILLING

ENGEO
Expect Excellence

Access the content of the ĪSSMGE Īnternational Journal of Geoengineering Case Histories at:
www.geocasehistoriesjournal.org

Downloaded: Saturday, November 14 2026, 01:53:48 UTC